

Rigorous bounds on the Analytic S-matrix

Andrea Guerrieri and Amit Sever

School of Physics and Astronomy, Tel Aviv University, Ramat Aviv 69978, Israel

We consider a dual S -matrix Bootstrap approach in $d \geq 3$ space-time dimensions which relies solely on the rigorously proven analyticity, crossing, and unitarity properties of the scattering amplitudes. As a proof of principle, we provide rigorous upper and lower numerical bounds on the quartic coupling for the scattering of identical scalar particles in four dimensions.

I. INTRODUCTION

An optimization problem can be viewed from either of two perspectives called respectively *Primal* and *Dual*.

In the revived non-perturbative S -matrix Bootstrap program of [1, 2], the space of scattering amplitudes is carved out numerically by solving an optimization problem in its *Primal* form: the target to optimize is a physical observable; the constraints are the physical principles of analyticity, crossing, and unitarity. This approach has already been used to bound several classes of amplitudes. For example, in relation to integrable systems in two dimensions [3–12], and in higher dimensions for the case of standard model physics [13–17] and quantum gravity theories [18]. At the same time, any bootstrap scheme in terms of the primal variables involves making an ansatz for the amplitude and some type of truncation: as a result, the bounds are not strictly rigorous.

Our main motivation for constructing a dual formulation stems from the *weak duality principle*. Suppose we maximize an observable \mathcal{O} over some space D . Then for any value of the dual variables in the dual space \bar{D} , the dual function $\bar{\mathcal{O}}$ will always provide an upper bound on \mathcal{O} , independently of how hard the primal problem is

$$\mathcal{O} \leq (\mathcal{O}_* \equiv \max_D \mathcal{O}) \leq (\bar{\mathcal{O}}_* \equiv \min_{\bar{D}} \bar{\mathcal{O}}) \leq \bar{\mathcal{O}}. \quad (1)$$

This weak duality principle allows one to construct a bootstrap scheme for generating rigorous bounds on the S -matrix, thus placing it in a similar footing to the Conformal Bootstrap [19]. In this letter, we formulate a dual S -matrix Bootstrap problem in $d \geq 3$ for the scattering of identical scalar particles that can be efficiently solved using SDPB [20, 21]. A closely related – albeit non-linear – formulation was pioneered long ago in a series of papers [22–26] and used to put rigorous bounds on the $\pi^0\pi^0$ scattering amplitude in four dimensions. Moreover, an alternative dual formulation has been constructed recently using the Mandelstam representation [27] – see also [9, 11, 28] for previous examples in two dimensions.

Before illustrating our strategy, we shall review the logic behind the dual approach in a simpler example.¹

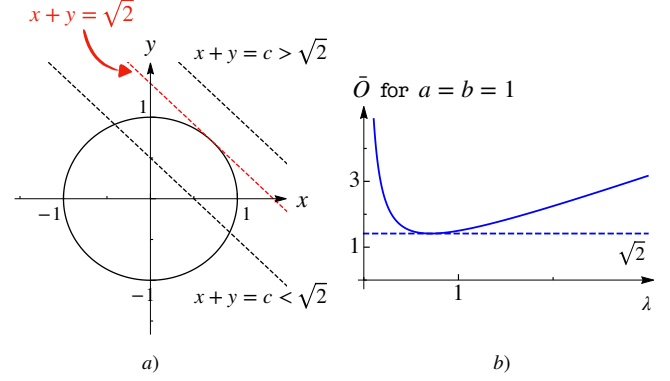


FIG. 1. a) The geometric solution of problem $\max \{x+y \mid x^2 + y^2 \leq 1\}$. b) The dual function $\bar{\mathcal{O}}(\lambda) = \lambda + 1/(2\lambda)$ of the same maximization problem. The minimum value is attained for $\lambda = 1/\sqrt{2}$ and coincides with the optimal value of the maximization problem.

We consider the following toy problem ²

$$\mathcal{O}_* \equiv \max_{\{x,y\}} \{\mathcal{O}(x,y) \mid x^2 + y^2 \leq 1\}, \quad (2)$$

with the *primal objective* taken to be

$$\mathcal{O}(x,y) = ax + by. \quad (3)$$

The (real) variables $\{x,y\}$ are called *primal variables*. The starting point to derive the dual version of problem (2) is to write the Lagrangian function

$$\mathcal{L}(x,y|\lambda) \equiv (ax + by) + \lambda(1 - x^2 - y^2), \quad (4)$$

introducing a *dual variable* for each constraint, as $\lambda \geq 0$. This Lagrangian satisfies the following identity

$$\min_{\lambda} \{\mathcal{L}|\lambda \geq 0\} = \begin{cases} ax + by & x^2 + y^2 \leq 1 \\ -\infty & \text{otherwise} \end{cases}. \quad (5)$$

Combining this with the *max-min inequality* yields

$$\begin{aligned} \mathcal{O}_* &\equiv \max_{\{x,y\}} \left\{ \min_{\lambda} \{\mathcal{L}|\lambda \geq 0\} \right\} \\ &\leq \min_{\lambda} \left\{ \bar{\mathcal{O}}(\lambda) \mid \lambda \geq 0 \right\} \equiv \bar{\mathcal{O}}_*, \end{aligned} \quad (6)$$

¹See Chapter 5 of [29] for a general introduction to dual problems.

²You may think of the objective to maximize as the representative of a physical observable and the constraint a toy version of unitarity.

where the *dual function* is defined as

$$\bar{O}(\lambda) \equiv \max_{\{x,y\}} \mathcal{L} = \lambda + (a^2 + b^2)/(4\lambda). \quad (7)$$

The last inequality in (6) proves the weak duality principle anticipated in (1).³

The dual objective in (7) is non-linear, but it is concave.⁴ For any fixed trial value of $\lambda \geq 0$ the dual function provides a rigorous upper bound for the quantity $ax + by$ of our toy problem. The difference between primal and dual objective is called *duality gap* and whether the duality gap is zero depends on the nature of the primal constraints.⁵

In the following, we will apply this same logic to bound the quartic coupling between identical massive scalar particles in d -dimensions, showing explicit numerical results for $d = 4$. We view our construction as a proof of principle that may be improved and optimized in the future.

II. THE QUARTIC COUPLING PROBLEM

We list the set of constraints for the $2 \rightarrow 2$ scattering amplitude of identical scalars. First, the analyticity of the amplitude in the cut s -plane can be imposed using dispersion relations. The amplitude satisfies fixed- t double subtracted dispersion relations for any real $-28 < t < 4$ in the s -plane with two cuts starting at $s = 4$ and $u = 4$, all expressed in units of the mass, [32–34]. Once combined with $s - u$ crossing, they can be put in the following form [34]⁶

$$0 = \mathcal{A}(s, t) = T(s, t) - T(s_0, t_0) - \frac{1}{\pi} \int_4^\infty dv [T_v(v, t)K(v, s, t; t_0) + T_v(v, t_0)K(v, t, t_0; s_0)], \quad (8)$$

where $T_v(v, t) = \text{Disc}_v T(v, t)$, and (s_0, t_0) is an arbitrary subtraction point. Here,

$$K(v, s, t; t_0) = \frac{1}{v-s} + \frac{1}{v-4+s+t} - \frac{1}{v-t_0} - \frac{1}{v-4+t+t_0}. \quad (9)$$

A function that satisfies the \mathcal{A} constraint is automatically analytic in the cut s -plane and $s - u$ crossing symmetric, but not necessarily $s - t$ symmetric. Hence,

this equation must be supplemented by the crossing constraint, $T(s, t) = T(s, 4 - s - t)$. This implies that the primal variables must consist of $s - t$ crossing symmetric functions, which in turn supports only even spins.⁷

Unitarity is most simply expressed as the probability conservation for fixed energy s and spin ℓ

$$1 = \sum_n |S_{2 \rightarrow n}(s, \ell)|^2 \geq |S_{2 \rightarrow 2}(s, \ell)|^2, \quad (10)$$

where $S_{2 \rightarrow n}(s, \ell)$ denotes the matrix element between 2-particle and n -particle states of spin ℓ . The $S_{2 \rightarrow 2}$ amplitudes are given by

$$S_{2 \rightarrow 2}(s, \ell) = 1 + i\rho^2(s)f_\ell(s), \quad (11)$$

where $\rho^2(s) = \frac{(s-4)^{\frac{d-3}{2}}}{\sqrt{s}}$ is the d -dimensional two-particle phase space factor and $f_\ell(s)$ the partial wave projection⁸

$$f_\ell(s) = \frac{\mathcal{N}_d}{2} \int_{-1}^1 dz (1 - z^2)^{\frac{d-4}{2}} P_\ell^{(d)}(z) T(s, t(z)), \quad (12)$$

with $t(z) = \frac{1}{2}(s-4)(z-1)$. For later convenience, we rephrase the unitarity constraint as the semi-definite (SDP) condition

$$\mathcal{U}_\ell(s > 4) = \begin{pmatrix} 1 - \frac{\rho^2}{2} \text{Im} f_\ell & \rho \text{Re} f_\ell \\ \rho \text{Re} f_\ell & 2 \text{Im} f_\ell \end{pmatrix} \succeq 0. \quad (13)$$

The equivalence between (10) and (13) can be seen by first noting that \mathcal{U}_ℓ is positive iff both its determinant and trace are positive. The positivity of the determinant is (10). The positivity of the trace for $s > 4$ follows from that of the determinant, as can be seen by noting that $\det \mathcal{U}_\ell = 2 \text{Im} f_\ell \text{tr} \mathcal{U}_\ell - 4 \text{Im} f_\ell^2 - \rho^2 \text{Re} f_\ell^2$.

Finally, in the elastic region of $4 < s < 16$, unitarity implies a stronger equality constraint

$$\det \mathcal{U}_\ell(16 > s > 4) = 0, \quad (14)$$

instead of the inequality (13).

The quantity we want to bound is the quartic coupling, defined as the value of the amplitude at the crossing symmetric point [2]

$$g_0 \equiv \frac{1}{2n_0^{(d)}} T\left(\frac{4}{3}, \frac{4}{3}\right). \quad (15)$$

³The case of a strong equality constraint, such as $(x^2 + y^2 := 1) = (x^2 + y^2 \leq 1) \wedge (x^2 + y^2 \geq 1)$, can equally be formulated in this form using two dual variables or equivalently, a single standard unconstrained Lagrange multiplier.

⁴This is always true for the dual problem, even when the primal problem is non-convex. It follows from the fact that the Lagrangian is an affine function of the dual variables and that the point-wise supremum operation preserves convexity. However, for non-convex problems, the duality gap does not necessarily close.

⁵See [29–31] for a set of sufficient conditions.

⁶See appendix A for a detailed derivation.

⁷Instead of imposing crossing as a constraint, one may use the manifestly crossing symmetric dispersion relations of [35, 36]. We leave this possibility to a future exploration [37].

⁸We work in the normalization of [38] in which $P_\ell^{(d)}(z) = {}_2F_1(-\ell, \ell + d - 3, (d - 2)/2, (1 - z)/2)$ and $\mathcal{N}_d = \frac{(16\pi)^{(2-d)/2}}{\Gamma((d-2)/2)}$. In this normalization, the orthogonality of the partial waves takes the form $\frac{\mathcal{N}_d}{2} \int_{-1}^1 dz (1 - z^2)^{\frac{d-4}{2}} P_\ell^{(d)}(z) P_{\ell'}^{(d)}(z) = \delta_{\ell\ell'} n_\ell^{(d)}$, with $n_\ell^{(d)} = \frac{(4\pi)^{\frac{d}{2}} (d+2\ell-3) \Gamma(d+\ell-3)}{\pi \Gamma((d-2)/2) \Gamma(\ell+1)}$.

Combining all the constraints, we write the Lagrangian

$$\mathcal{L}^\pm = g_0 + \iint_{\mathcal{D}} ds dt \mathcal{W}(s, t) \mathcal{A}(s, t) \quad (16)$$

$$+ \sum_{\ell \text{ even}} \left[\int_4^{16} ds E_\ell(s) \det \mathcal{U}_\ell(s) \pm \int_4^\infty ds \text{tr}(\mathbf{\Lambda}_\ell(s) \mathcal{U}_\ell(s)) \right],$$

where $\mathcal{W}(s, t)$ and $E_\ell(s)$ are unconstrained dual variables imposing the analyticity (8) and elastic unitarity (14) in their validity domains, \mathcal{D} and $s \in [4, 16]$. Here, crossing has already been solved at the level of the primal variables by restricting to even spins only, $f_{2n+1}(s) = 0$. Finally, $\mathbf{\Lambda}_\ell(s)$ is a semidefinite positive matrix associated to the unitarity inequality constraint (13) that we impose for all energies.¹⁰

A. The dual variable space

Here comes the important advantage of the dual formulation: omitting part of the constraints may weaken the bound, but due to the inequality $\min_\lambda \{\bar{\mathcal{O}}(\lambda)\} \leq \bar{\mathcal{O}}(0)$, it does not affect its rigor.

First, we simply set the dual variables associated with the elastic unitarity constraint (14) to zero, $E_\ell(s) = 0$. This is because we do not know how to put it in SDP form. In the end, we find the elastic unitarity is satisfied in the region where the unitarity inequality is imposed – see also sec. II C.¹¹

Next, we discuss the dual function $\mathcal{W}(s, t)$. Its analyticity properties are connected to those of its associated constraint $\mathcal{A}(s, t)$ and its domain of validity. We consider a sub-space of dual functions whose s -channel spin is bounded by a fixed integer L

$$\mathcal{W}_L(s, t(z)) = \frac{\mathcal{N}_d}{2} (1-z^2)^{\frac{d-4}{2}} \sum_{\ell=0}^L w_\ell(s) P_\ell^{(d)}(z), \quad (17)$$

where the sum runs over all spins, even and odd. Note that even though we have solved the crossing constraint at the level of the primal variables by setting $f_{2n+1}(s) = 0$, the odd spins dual variables $w_{2n+1}(s)$ impose non-trivial constraints. This is because the kernel in (8) is not $s-t$ symmetric.

At this point, we shall specify the domain \mathcal{D} of \mathcal{W}_L where we impose the \mathcal{A} -constraint. The larger this domain is, the more constraints we are imposing, hence the

stronger is the bound we get. The regime of validity of \mathcal{A} is $-28 < t < 4$ and any s . In addition, we demand the integral of $\mathcal{W}(s, t) T(s, t)$ in (16) to be diagonal in spin. This is achieved by letting z run over the range $z \in [-1, 1]$.

Combining the two conditions above implies that $0 < s < 32$. All in all, we take the integration domain to be $\mathcal{D}_\mu = \{(s, z) | z \in [-1, 1] \wedge s \in [4, \mu^2]\}$, where $4 < \mu^2 < 32$ is a free parameter that we will tune later when solving the dual problem numerically. Later we will also comment about the possibility of enlarging further this integration domain – see Sec. II B.

With these choices, the \mathcal{A} -term in the Lagrangian (16) takes the form

$$\iint_{\mathcal{D}_\mu} ds dt \mathcal{W}_L(s, t) \mathcal{A}(s, t) = \sum_{\ell=0}^L \int_4^{\mu^2} ds w_\ell(s) a_\ell(s), \quad (18)$$

where

$$a_\ell(s) \equiv \frac{\mathcal{N}_d}{2} \int_{-1}^1 dz (1-z^2)^{\frac{d-4}{2}} P_\ell(z) \mathcal{A}(s, t(z)) = \quad (19)$$

$$\text{Re } f_\ell(s) - \frac{\delta_{\ell,0}}{n_0^{(d)}} T(s_0, t_0) - \int_4^\infty dv \sum_{J \text{ even}} k_{\ell,J}(v, s) \text{Im } f_J(v),$$

with the kernels $k_{\ell,J}$ given by

$$k_{\ell,J}(v, s) \equiv \frac{\mathcal{N}_d n_J^{(d)}}{2\pi} \int_{-1}^1 dz (1-z^2)^{\frac{d-4}{2}} P_\ell^{(d)}(z) \quad (20)$$

$$\times \left[P_J(1 + \frac{2t}{v-4}) K(v, s, t; t_0) + P_J(1 + \frac{2t_0}{v-4}) K(v, t, t_0; s_0) \right].$$

In (19) we used the fact that the imaginary part of the \mathcal{A} -constraint is automatically satisfied for real $s > 4$. The even spin constraints $a_{2n}(s) = 0$ are also known as *Roy equations* [34]. They relate the real part of each partial amplitude to the absorptive parts that can be measured experimentally and they have been successfully used in low energy QCD phenomenology, see [40] for a review. Notice also that the odd constraints $a_{2n+1}(s) = 0$ do not contain the odd spin real parts as we set $\text{Re } f_{2n+1}(s) = 0$ by the choice of the primal variables.

B. The dual problem

By plugging (18) into (16), and choosing conveniently the subtraction point at $s_0=t_0=4/3$, the Lagrangian becomes

$$\mathcal{L}^\pm = g_0 \left(1 - 2 \int_4^{\mu^2} w_0(s) ds \right) + \sum_{\ell=0}^L \int_4^{\mu^2} ds w_\ell(s) \text{Re } f_\ell(s) \quad (21)$$

$$- \int_4^\infty dv \sum_{J \text{ even}} \bar{w}_J(v) \text{Im } f_J(v) \pm \int_4^\infty dv \sum_{J \text{ even}} \text{tr}(\mathbf{\Lambda}_J(v) \mathcal{U}_J(v)),$$

⁹The sign \pm depends on whether we want to maximize or minimize g_0 .

¹⁰A simple theorem states that the integrand $\text{tr}(\mathbf{\Lambda}_\ell(s) \mathcal{U}_\ell(s))$ is positive iff $\mathcal{U}_\ell(s) \succeq 0$ for any $\mathbf{\Lambda}_\ell(s) \succeq 0$.

¹¹It can be shown on general grounds that even with $E_\ell(s) = 0$, the Lagrangian (16) leads to elastic functions, see [26] and appendix D. This is not in contradiction with the Ask theorem, [39], because the S-matrix constraints are not imposed to an arbitrary large s .

where

$$\bar{w}_J(v) \equiv \sum_{\ell=0}^L \int_4^{\mu_e^2} ds w_\ell(s) k_{\ell,J}(v, s). \quad (22)$$

Before moving to the dual problem, we observe that using the symmetry $z \rightarrow -z$ of the even spin partial waves $f_{2n}(s)$, we can extend the integration domain of the even spins w_{2n} in the definition of (22) up to $\mu_e^2 \leq 60$. This is achieved by integrating over half of the angles $z \in [0, 1]$ in (19) and compensating by an overall factor of 2. The region of integration for the odd spins is kept up to $\mu_o^2 \leq 32$. In the next section and appendix E we will find that having $w_{2n}(s > 12) \neq 0$ and $w_{2n+1}(s > 8) \neq 0$ is not feasible, so in practice one is forced to take $\mu_e^2 \leq 12$ and $\mu_o^2 \leq 8$. Yet, the $z \rightarrow -z$ symmetry is what allows the even spins bound to be larger than the odd one.

As in the toy problem (2), we define the dual functional by maximizing (minimizing) \mathcal{L}^+ (\mathcal{L}^-) over the primal variables. The Lagrangian is linear in the primal variables and the extremization tedious, but straightforward – see appendix B for the details. The final result is

$$\min_{\substack{\Lambda_J^\pm \succeq 0 \\ \pm \bar{w}_J(s) \geq 0}} \pm D^\pm \equiv \min_{\substack{\Lambda_J^\pm \succeq 0 \\ \pm \bar{w}_J(s) \geq 0}} \sum_{n=0}^{\lfloor L/2 \rfloor} \int_4^{\mu_e^2} ds X_{2n}(s), \quad (23)$$

where J is an even spin. Here, Λ_J is the dual matrix that is associated with the unitarity constraint. It is given by

$$\Lambda_J^\pm = \begin{pmatrix} X_J & \mp \frac{w_J}{2\rho} \\ \mp \frac{w_J}{2\rho} & \frac{1}{4}(\rho^2 X_J \pm 2\bar{w}_J) \end{pmatrix} \succeq 0. \quad (24)$$

In (23) this constraint is imposed for $4 < s < \mu_e^2$ and $0 \leq J \leq L$. In the complementary set, the following linear constraints are imposed

$$\pm \bar{w}_{J \leq L}(s > \mu_e^2) \geq 0, \quad \pm \bar{w}_{J > L}(s > 4) \geq 0. \quad (25)$$

Finally, the dual variable w_0 shall be normalized to

$$\int_4^{\mu_e^2} ds w_0(s) = \frac{1}{2}. \quad (26)$$

C. Numerical results

We have implemented the dual problem (23-26) in $d = 4$ numerically. The summary of this investigation together with the one for the primal problem is plotted in figure 2. In red we depict the rigorously excluded region for g_0 . In green, the allowed region obtained using primal numerics is indicated for comparison.

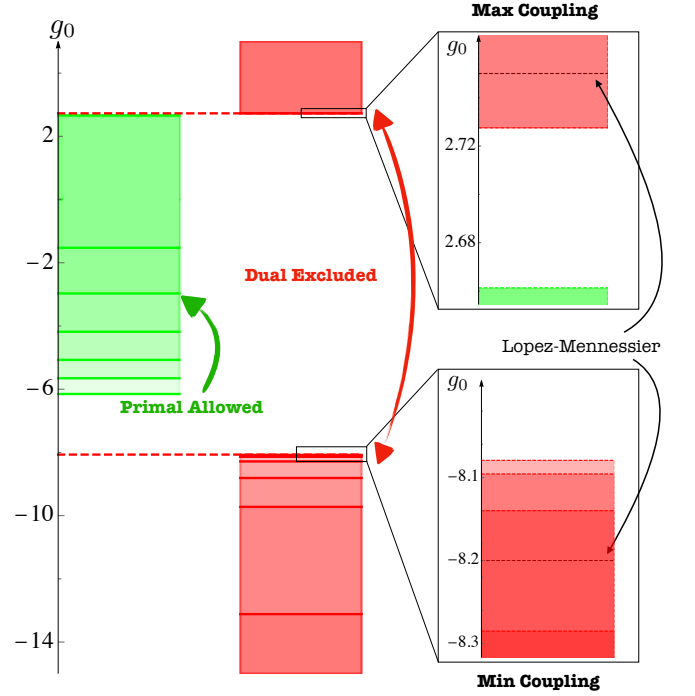


FIG. 2. Bounds on the quartic coupling g_0 . On the left, we show in green the region determined by solving the primal problem, in red the one rigorously excluded by solving the dual (23). The bound on the maximum coupling converges fast both in the primal and dual problem and the gap is relatively small, though non-vanishing – right-top inset. The bound on the minimum coupling is hard to study using primal: the different green lines denote the numerical coupling for $N_{\max} = 5, 8, 11, 14, 17, 20$. On the contrary, the red lines for $L = 0, \dots, 6$ show that dual convergence is achieved faster – right-bottom inset. In dashed black we report the best values of [26].

Primal - We solve the primal problem by considering a manifestly crossing symmetric ansatz of the form

$$T^{\text{primal}}(s, t, u) = \frac{c}{\rho_s - 1} + \sum_{a+b \leq N_{\max}} c_{(ab)} \rho_s^a \rho_t^b + \text{symm}, \quad (27)$$

with $\rho_x = (\sqrt{8/3} - \sqrt{4-x})/(\sqrt{8/3} + \sqrt{4-x})$ and by imposing unitarity numerically up to some spin L_{\max} on a grid of points. For the maximum coupling case, convergence is remarkably fast. Conversely, the minimum coupling convergence is terrible: the different green lines in figure 2 correspond to increasing values of N_{\max} indicating that primal convergence is far from being attained.

Dual - The functional constraints (23-26) are implemented as follows. The dual variables X_{2n} and w_ℓ for $n = 0, \dots, \lfloor L/2 \rfloor$ and $\ell = 0, \dots, L$ are parametrized using a simple basis of functions that we took to be the Chebyshev polynomials. We then choose a grid of points where we impose (24) and (25), see appendix G for details.

The set of constraints (25) on the sign of $\bar{w}_{J > L}$ is how-

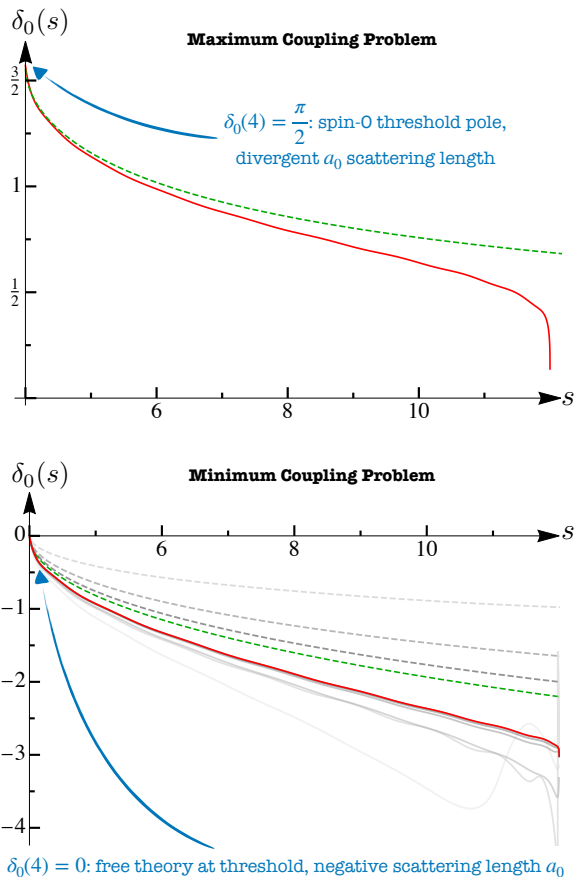


FIG. 3. The spin-0 phase shifts, $\delta_0 = \frac{1}{2i} \log S_0$, as a function of the center of mass energy s for the maximum (top) and minimum coupling (bottom). We plot in dashed-green and solid-red the phase shifts obtained respectively from the best primal and dual numerics. In the bottom figure, the dashed lines in gray-scale correspond to increasing values of N_{\max} up to $N_{\max} = 20$ (in green); the solid lines in gray-scale are obtained from the dual for different values of L , up to $L = 6$ (in red). Although primal and dual results still differ, the physical content they describe is the same, converging one towards the other as the duality gap shrinks.

ever infinite because the spin is unbounded. To implement them numerically, we first trivialize them at large J . This leads to a bound on the integration domain $\mu_e^2 \leq 12$, $\mu_o^2 \leq 8$ – see appendix E for the details. We then introduce a spin cutoff J_{\max} on the set (25) and gradually increase it. At intermediate spins larger than J_{\max} we have also implemented the sign constraint near the two-particle threshold, see appendix F. For the maximal coupling problem, we observe that beyond a certain value there are no dual constraint violations. For the minimal coupling problem, we always have some tiny violations at some $J > J_{\max}$, hows effect on the bound is negligible.

For the dual maximum coupling the simplicity of the primal mirrors into the dual. An almost optimal bound is attained using just $L = 0$, and adding further dual variables w_ℓ does not improve significantly the bound. For the minimum coupling, the dual numerical convergence

is relatively slower as in the primal case. The red lines in figure 2 are obtained adding multipliers from $L = 0$ up to $L = 6$. However, we stress again that for any fixed L the bounds obtained with large J_{\max} convergence are rigorous. Increasing further L will possibly make the duality gap smaller.¹²

The different convergence rate of the two problems can be understood as follows. The quartic coupling g_0 can be measured using the dispersion relation $\mathcal{A}(4, 0)$ in (8) subtracting at $s_0 = t_0 = 4/3$

$$32\pi g_0 = \text{Re } T(4, 0) - \frac{1}{\pi} \int_4^\infty dv [T_v(v, 0) K(v, 4, 0; 4/3) + T_v(v, 4/3) K(v, 0, 4/3; 4/3)]. \quad (28)$$

The integrand on the right hand side is positive since $T_v(v, t_0) \geq 0$ for any $t_0 \geq 0$. From (28) it is evident that maximizing the coupling is equivalent to minimizing the imaginary part (or the total cross-section). On the other hand, when we minimize g_0 the optimal solution will have a total cross-section that is as big as possible compatibly with unitarity. In this sense it is not surprising that primal convergence for the minimum coupling case is so hard since the imaginary part of our ansatz (27) does not grow at fixed N_{\max} .¹³

In figure 3 we compare the primal and dual spin-0 phase shift for the maximum and minimum coupling problem. The phase shifts for both problems tend to differ less as the duality gap shrinks. Moreover, it is encouraging to notice they have the same threshold behavior: the amplitude saturating the maximum coupling has a threshold singularity; the one saturating the minimum coupling a negative scattering length – see appendix H for further details.

III. DISCUSSION AND OUTLOOK

In this Letter, we proposed a dual approach to the S -matrix Bootstrap based solely on the proven analyticity properties of scattering amplitudes.¹⁴ Our strategy consists of decomposing both crossing and unitarity into simpler constraints that can be systematically added to improve the bounds.

Still, there are some important questions to address. The first one concerns the duality gap. The dual problem we optimized numerically (23) is not the ‘mathematical dual’ of the primal problem we solved following [6] and the duality gap does not necessarily close. In particular, in the dual, we imposed full unitarity up to $s = 12$.

¹²See appendix G for a detailed analysis of the dual numerics.

¹³It might be worth investigating whether the amplitude minimizing the quartic coupling also saturates the Froissart bound in $d = 4$.

¹⁴See [41, 42] for a recent derivation of crossing symmetry using on-shell methods.

This limitation follows from the dispersion relations we assumed in (8).¹⁵ It might be interesting to use more refined dispersion relations [37] and check whether the gap can be further shrunk. In particular, it would be interesting to extend the applicability of the dual method beyond $s = 16$, where non-elasticity is expected to kick in.

Although not proven, maximal analyticity is a typical working assumption made in bootstrap studies. It would be worth repeating our analysis under such a hypothesis and compare it with our rigorous bounds. It would also be interesting to extend the dual formulation to the case of massless particles. Clearly, in that case, the validity regime of our formulation shrinks to zero and some assumptions are needed in order to make progress. Related to that, it would be important to generalize the dual problem we formulated to bound Wilson coefficients in EFTs that recently has received a lot of attention [47–54].

Finally, one of the hardest challenges in the S -matrix Bootstrap program concerns the inclusion of multi-particle processes. The proliferation of Mandelstam invariants is the bottleneck of manifestly crossing symmetric approaches. Single variable dispersion relations can overcome this issue. Whether the dual technology developed in this Letter can be used to tackle such challenging problems is an open question we think it will be important to address.

ACKNOWLEDGMENTS

We thank M. Correia, J. Elias-Miró, A. Homrich, J. Penedones, A. Raclariu, P. Vieira, and A. Zhiboedov for useful discussion. We thank P. Vieira for comments on the draft. AG was supported by The Israel Science Foundation (grant number 2289/18). AS was supported by the Israel Science Foundation (grant number 1197/20).

Appendix A: Fixed- t dispersion relations

In this appendix, we give a derivation of the fixed- t dispersion relation with two subtractions in (8). For real $t < 4$ the amplitude is polynomially bounded by $(s/s_0)^2$, [33]. Hence, there are only two subtractions needed for a dispersion representation. It is useful to perform these subtractions using a simple division by s^2 . In that way,

we arrive at

$$\begin{aligned} T(s, t) &= \frac{s^2}{2\pi i} \oint \frac{dv}{v-s} \frac{T(v, t)}{v^2} \\ &= T(0, t) + s T'(0, t) + \frac{s^2}{\pi} \int_4^\infty \frac{dv}{v-s} \frac{T_s(v, t)}{v^2} \\ &\quad + \frac{s^2}{\pi} \int_{-\infty}^{-t} \frac{dv}{v-s} \frac{T_v(v, t)}{v^2} \\ &= T(0, t) + s T'(0, t) + \frac{s^2}{\pi} \int_4^\infty \frac{dv}{v-s} \frac{T_v(v, t)}{v^2} \\ &\quad + \frac{s^2}{\pi} \int_4^\infty \frac{dv}{v-u} \frac{T_v(v, t)}{(4-t-v)^2} \end{aligned} \quad (\text{A1})$$

where $T'(0, t) = \partial_v T(v, t)|_{v=0}$ and $T_s(s, t) = \text{Disc}_s T(s, t)$, and in the second step we have used crossing symmetry. This t -channel dispersion integral representation is however not manifestly $s \leftrightarrow u$ crossing symmetric. To make this symmetry manifest, we express the integral as

$$\begin{aligned} T(s, t) &= T(0, t) + s T'(0, t) + 2 \frac{s^2}{\pi} \int_4^\infty \frac{dv}{v-s} \frac{T_v(v, t)}{v^2} \\ &\quad + \frac{s^2}{\pi} \int_4^\infty dv T_v(v, t) \left[\frac{1}{(v-u)(4-t-v)^2} - \frac{1}{(v-s)v^2} \right]. \end{aligned}$$

After averaging this with the u -channel we arrive at [34]

$$T(s, t) = g(t) + \frac{1}{\pi} \int_4^\infty dv \frac{T_v(v, t)}{v^2} \left[\frac{s^2}{v-s} + \frac{u^2}{v-u} \right], \quad (\text{A2})$$

where

$$g(t) = T(0, t) + \frac{4-t}{2} T'(0, t) + \frac{1}{2\pi} \int_4^\infty dv \frac{T_v(v, t)}{v^2} \frac{(4-t)^3}{(4-t-v)^2}. \quad (\text{A3})$$

Next, we want to trade $g(t)$ for a known function of t and an unknown subtraction constant. We use first the crossing equation $T(t, t_0) = T(t_0, t)$ to eliminate $g(t)$ in terms of $g(t_0)$ with $0 < t_0 < 4$

$$\begin{aligned} g(t) &= g(t_0) - \frac{1}{\pi} \int_4^\infty dv \frac{T_v(v, t)}{v^2} \left(\frac{t_0^2}{v-t_0} + \frac{(4-t-t_0)^2}{v-4+t_0+t} \right) \\ &\quad - \frac{1}{\pi} \int_4^\infty dv \frac{T_v(v, t_0)}{v^2} \left(\frac{t^2}{v-t} + \frac{(4-t-t_0)^2}{v-4+t_0+t} \right), \end{aligned} \quad (\text{A4})$$

and then using the definition of $T(s_0, t_0)$ with $0 < s_0 < 4$ (so that $T(s_0, t_0)$ is real) we eliminate also $g(t_0)$, obtaining the equation in (8).

Note that a function that satisfies this $\mathcal{A}(s, t) = 0$ constraint is manifestly $s \leftrightarrow u$ crossing symmetric, but not necessarily $s \leftrightarrow t$ symmetric.

¹⁵After Roy's papers other authors have tried to further extend the domain of validity of the Roy equations [36, 43, 44], see [45, 46] for recent studies.

Appendix B: Derivation of the SDP problem

In this appendix we derive the dual problem (23)-(26) by extremizing the Lagrangian (21) over the primal variables, $f_\ell(s)$, and some of the components of the dual variables $\Lambda_J(s)$.

The integrand of the unitarity term can be expanded as

$$\text{tr}(\Lambda_J(s)\mathcal{U}_J(s)) = 2 \text{Im } f_J(s) \Lambda_J^{22}(s) + 2 \text{Re } f_J(s) \rho^2(s) \Lambda_J^{12}(s) + \Lambda_J^{11}(s) (1 - \rho^2(s) \text{Im } f_J(s)/2). \quad (\text{B1})$$

Extremizing (21) w.r.t. the primal variables yields the equations

$$\begin{aligned} (\Lambda_J^{22})^\pm &= [\rho^2(s) \Lambda_J^{11}(s) \pm 2\bar{w}_J(s)] / 4, \\ (\Lambda_J^{12})^\pm &= \begin{cases} \mp \frac{w_J(s)}{2\rho(s)} & (4 < s < \mu_e^2) \wedge (\text{even } J \leq L) \\ 0 & \text{otherwise} \end{cases}. \end{aligned} \quad (\text{B2})$$

We use these equations to eliminate Λ_J^{12} and Λ_J^{22} . After this choice, the Lagrangian takes the form

$$D^\pm(s_0, t_0) \equiv \pm \sum_{J \text{ even}} \int_4^{\mu_e^2} ds X_{2n}(s), \quad (\text{B3})$$

where $X_J(s) \equiv \Lambda_J^{11}$. It is subject to the semi-definite positive condition

$$\Lambda_J^\pm(s) = \begin{pmatrix} X_J(s) & \mp \frac{w_J(s)}{2\rho(s)} \\ \mp \frac{w_J(s)}{2\rho(s)} & \frac{1}{4} (\rho^2(s) X_J(s) \pm 2\bar{w}_J(s)) \end{pmatrix} \succeq 0, \quad (\text{B4})$$

for $(4 < s < \mu_e^2) \wedge (J \leq L)$ and

$$\Lambda_J^\pm(s) = \begin{pmatrix} X_J(s) & 0 \\ 0 & \frac{1}{4} (\rho^2(s) X_J(s) \pm 2\bar{w}_J(s)) \end{pmatrix} \succeq 0, \quad (\text{B5})$$

otherwise. The equation of motion for g_0 results in the additional normalization condition (26).

At this point, the dual objective is still an infinite sum of dual variables, making the problem difficult to solve. However, the constraint in (B5) can be solved analytically by setting $X_J(s) = 0$ its domain of validity $((s > \mu_e^2) \wedge (J \leq L)) \vee ((s > 4) \wedge (J > L))$, and imposing the simpler linear conditions

$$\pm \bar{w}_J(s) \geq 0, \quad (\text{B6})$$

in this regime. This last step leads to the final formulation of the *Dual SDP Problem* quoted in the main text (23).

Appendix C: Derivation of the non-linear problem

In this appendix, we derive the dual problem by imposing unitarity in the form of the non-linear inequality

$\det \mathcal{U}_\ell(s) \geq 0$. This form has some conceptual advantages, but it is difficult to solve numerically. We will not use it for any systematic numerical exploration, but it will give us a procedure to extract the primal phase shifts from the dual SDP problem (23).

We start from the Lagrangian in (21) and replace the SDP unitarity constraint by its non-linear form

$$\text{tr}(\Lambda_J(s)\mathcal{U}_J(s)) \rightarrow \lambda_J(s) (2 \text{Im } f_J(s) - \rho^2 |f_J(s)|^2).$$

The equation of motions for the primal variables $\text{Re } f_J$ and $\text{Im } f_J$ yield

$$\begin{aligned} \text{Im } f_J(s) &= \frac{1}{\rho^2(s)} \mp \frac{\bar{w}_J(s)}{2\rho^2(s)\lambda_J(s)}, \\ \text{Re } f_J(s) &= \pm \begin{cases} \frac{w_J(s)}{2\rho^2(s)\lambda_J(s)} & (4 < s < \mu_e^2) \wedge (\text{even } J \leq L) \\ 0 & \text{otherwise} \end{cases} \end{aligned} \quad (\text{C1})$$

As before, the equation of motion for g_0 implies (26).

By plugging the solution (C1) into the Lagrangian we arrive at the dual function

$$\begin{aligned} \mathcal{D}^\pm(s_0, t_0) &\equiv \pm \sum_{n=0}^{\lfloor L/2 \rfloor} \int_4^{\mu_e^2} dv \frac{w_{2n}^2(v)}{4\rho^2(v)\lambda_{2n}(s)} \\ &\quad \pm \sum_{J \text{ even}} \int_4^\infty dv \frac{(\bar{w}_J(v) \mp 2\lambda_J(v))^2}{4\rho^2(s)\lambda_J(s)}. \end{aligned} \quad (\text{C2})$$

The dual unitarity variables $\lambda_J(s)$ are unconstrained positive functions and they appear quadratically in the dual objective. It is, therefore, possible to find the extremum of this action analytically w.r.t. λ_J .

For $4 < s < \mu_e^2$ and $J \leq L$ we get

$$\lambda_J(s) = \frac{1}{2} \sqrt{w_J^2(s) + \bar{w}_J^2(s)} \geq 0, \quad (\text{C3})$$

and in the complementary region

$$\lambda_J(s) = \mp \frac{1}{2} \bar{w}_J(s), \quad \lambda_J(s) \geq 0. \quad (\text{C4})$$

Plugging the solution (C3) and (C4) into the dual action yields

$$\begin{aligned} \tilde{\mathcal{D}}^\pm(s_0, t_0) &\equiv \sum_{n=0}^{\lfloor L/2 \rfloor} \int_4^{\mu_e^2} ds \frac{(-\bar{w}_{2n}(s) \pm \sqrt{w_{2n}^2(s) + \bar{w}_{2n}^2(s)})}{\rho^2(s)} \\ &\quad - \sum_{n=0}^{\lfloor L/2 \rfloor} \int_{\mu_e^2}^\infty ds \frac{2}{\rho^2(s)} \bar{w}_{2n}(s) \theta(\mp \bar{w}_{2n}(s)) \\ &\quad - \sum_{n > \lfloor L/2 \rfloor} \int_4^\infty ds \frac{2}{\rho^2(s)} \bar{w}_{2n}(s) \theta(\mp \bar{w}_{2n}(s)). \end{aligned} \quad (\text{C5})$$

The dual problem in terms of $\tilde{\mathcal{D}}^\pm$ is nonlinear and unconstrained modulo the spin zero normalization condition (26). However, the presence of the step function

makes this non-linear formulation challenging to solve using gradient methods.¹⁶

The dual objective (C5) can be further simplified by imposing the inequality $\pm \bar{w}_J(s) \geq 0$ on the support of the θ functions. Then the θ functions contributions can be neglected and this is consistent respectively with the minimization/maximization of $\tilde{D}^\pm(s_0, t_0)$. These conditions coincide with those we find in the SDP case (B6). The non-linear dual problem for the quartic coupling becomes

$$\begin{aligned} & \min \pm \tilde{D}^\pm(s_0, t_0) \\ & = \min \sum_{n=0}^{\lfloor L/2 \rfloor} \int_4^{\mu_e^2} ds \frac{\mp \bar{w}_{2n}(s) + \sqrt{w_{2n}^2(s) + \bar{w}_{2n}^2(s)}}{\rho^2(s)}, \end{aligned} \quad (\text{C6})$$

subject to the constraints (B6).

The problem (C6) depends on a finite number of dual functions $w_\ell(s)$ for any $0 \leq \ell \leq L$, but it is non-linear and constrained. It would be important to develop an efficient numerical algorithm to solve this class of problems.

Appendix D: Phase shifts

In the SDP formulation of the Bootstrap problem (23), we cannot reconstruct the phase shifts once we extremize over the primal variables. On the other hand, in the non-linear formulation (C5), using the eqs. (C1) and (C3) it is straightforward to obtain

$$S_J^\pm(s) = 1 + i\rho^2(s)f_J^\pm(s) = \mp \frac{W_J^*}{|W_J|}, \quad W_J = iw_J - \bar{w}_J, \quad (\text{D1})$$

respectively for the maximum and minimum coupling problem and for $(4 < s < \mu_e^2) \wedge (0 \leq J \leq L)$.

It does not come as a surprise that the two problems are simply related since they were derived using different equivalent versions of the unitarity constraints. To understand their relation, we look at the dual unitarity constraints (B4). Suppose $\det \Lambda_J^\pm(s) = \epsilon^2 > 0$, then we can solve for $X_J > 0$ obtaining

$$X_J^*(s) = \frac{\pm \bar{w}_J + \sqrt{\bar{w}_J^2 + w_J^2 + \epsilon^2}}{\rho^2} \geq \frac{\pm \bar{w}_J + \sqrt{\bar{w}_J^2 + w_J^2}}{\rho^2} \quad (\text{D2})$$

The last inequality implies an inequality for the linear and non-linear dual objectives

$$|D^\pm(s_0, t_0)| \geq |\tilde{D}^\pm(s_0, t_0)|, \quad (\text{D3})$$

with the equality attained when $\epsilon = 0$, or equivalently, when $\det \Lambda_J^\pm(s) = 0$.

In that case, when $\epsilon = 0$, the two objectives coincide and we can use the definition (D1) and apply it to the numerical solution of our SDP problem. In practice, $\det \Lambda_\ell^\pm(s) \approx 0$ for all our numerical results – see figure 6 and figure 9 for a comparison between the reconstructed phase shifts using (D1) and the direct primal phase shifts.

Appendix E: Analytic constraints from asymptotic regimes

The sign constraints on the $\bar{w}_J(v)$ functionals (25) should be imposed to an arbitrary high spin. This is, of course, outside the scope of a numerical application. To overcome this difficulty, in this appendix we solve these constraints analytically at large spin. Doing so is crucial for our numerical implementation to converge into a solution that satisfies all the constraints at large J_{max} . We find that the large J constraints are only feasible if $\mu_e^2 \leq 12$ and $\mu_o \leq 8$. For simplicity, in this appendix, we set $d = 4$.

Recall the definition of $\bar{w}_J(v)$ in (22) that we repeat here for convenience

$$\bar{w}_J \equiv \sum_{n=0}^{\lfloor L/2 \rfloor} \int_4^{\mu_e^2} ds w_{2n} k_{2n, J} + \sum_{n=0}^{\lceil L/2 - 1 \rceil} \int_4^{\mu_o^2} ds \frac{w_{2n+1}}{2} k_{2n+1, J}, \quad (\text{E1})$$

where, $\mu_e^2 \leq 60$ and $\mu_o^2 \leq 32$. The dependence on J of $\bar{w}_J(v)$ only comes from the kernels

$$\begin{aligned} k_{\ell, J}(v, s) &= \frac{2J+1}{\pi} \int_{z_{\min}}^1 dz P_\ell(z) \times \\ & [P_J(x(v, t))K(v, s, t; t_0) + P_J(x(v, t_0))K(v, t, t_0; s_0)], \end{aligned} \quad (\text{E2})$$

where $z_{\min} = 0$ for ℓ even, $z_{\min} = -1$ when ℓ is odd, $t = t(z) = \frac{1}{2}(s-4)(z-1)$, and $P_\ell(z) = P_\ell^{(4)}(z)$ are the Legendre polynomials. To solve the constraint on \bar{w}_J at large J we will simplify (E2) into a single J -independent constraint. The range of v in which this constraint is imposed can be divided into two regions, inner and outer. In each of these regions one of the two terms in (E2) dominates over the other.

Consider the second term first. The constraint (25) is imposed for $v > 4$ and $t_0 = 3/4 > 0$. In this regime, the argument of the partial wave is larger than one, $x(v, t_0) = 1 + \frac{2t_0}{v-4} > 1$. At large J and for $x > 1$, the Legendre polynomials $P_J(x)$ grow exponentially as

$$P_J(x) = \frac{(x + \sqrt{x^2 - 1})^J}{\sqrt{2\pi J} \sqrt{1 + x(\sqrt{x^2 - 1} - x)}} (1 + \mathcal{O}(1/J)). \quad (\text{E3})$$

Hence, at large J and for a generic point where the kernel K does not have a zero or a pole, the second term in (E2)

¹⁶It is possible to replace an integrand of the form $-x\theta(-x)$ with its smooth approximation using the inequality $-x\theta(-x) = -x + \sqrt{x^2} \leq -x + \sqrt{x^2 + \epsilon^2}$ for some ϵ in order to use simple gradient algorithms. It might be worth exploring this possibility. A similar trick works also for $-x\theta(x)$.

dominate over the first, provided that $x(v, t_0) \geq |x(v, t)|$. Because $t(z) < 0$, this can fail only when

$$x(v, t(z)) = 1 + \frac{2t(z)}{v-4} = \frac{v-s+z(s-4)}{v-4} \leq -1. \quad (\text{E4})$$

The maximal value of $|x(v, t(z))|$ is archived at $z = z_{\min}$ and $s = \mu^2$. At the critical point v_c we have $x(v_c, t(z_{\min})|_{s=\mu^2}) = -x(v_c, t_0)$ and hence

$$v_c = 2 + \frac{\mu^2}{2} - t_0 - \frac{z_{\min}}{2}(\mu^2 - 4). \quad (\text{E5})$$

In general, v_c will be different for even and odd spins because of the different values of z_{\min} and μ^2 . However, if we choose the upper limit of integration for odd spins in (E1) to be $\mu_o^2 = 2 + \frac{\mu_e^2}{2}$, then v_c is the same and is given by

$$v_c = 2 + \frac{\mu_e^2}{2} - t_0. \quad (\text{E6})$$

As we now explain, making this choice will allow us to factor out the common J -dependant factor from the two terms in (E1). We denote the case where $v > v_c$, *outer region*, in which the term with $P_J(x(v, t_0))$ dominates the integral over z and s . In the *inner region*, $4 < v < v_c$, and the term with $P_J(x(v, t))$ dominates the integrals.

The above division into inner and outer regions of dominance can break down at points where one of the kernels in (E2) has a zero or a pole. However, because the partial waves are exponentially large, the contribution of such isolated points to the integral in (E2) is negligible.

1. Constraints from the outer region

In the outer region $v > v_c$ and at large J equation (E2) becomes

$$k_{\ell, J}(v, s) \sim \frac{2J+1}{\pi} P_J(x(v, t_0)) k_{\ell}^{\text{out}}(s, v), \quad (\text{E7})$$

with

$$k_{\ell}^{\text{out}}(s, v) = \int_{z_{\min}}^1 dz P_{\ell}(z) K(v, t(z), t_0; s_0). \quad (\text{E8})$$

Using the definition (E1), the functional \bar{w}_J in this region behaves as

$$\bar{w}_J(v) \sim \frac{2J+1}{\pi} P_J(x(v, t_0)) \bar{y}(v), \quad (\text{E9})$$

with

$$\bar{y}(v) \equiv \sum_{n=0}^{\lfloor L/2 \rfloor} \int_4^{\mu_e^2} ds w_{2n} k_{2n}^{\text{out}} + \sum_{n=0}^{\lfloor L/2-1 \rfloor} \int_4^{\mu_o^2} ds \frac{w_{2n+1}}{2} k_{2n+1}^{\text{out}}.$$

Because $x(v, t_0) > 1$, the sign constraint (25) reduces to the J -independent linear constraint $\pm \bar{y}(v) \geq 0$. We impose it for $v > v_c$ choosing a grid in v .

2. Constraints from the inner region

In the inner region $4 < v < v_c$ the large J behaviour of \bar{w}_J is more subtle because $x(v, t(z))$ dependence on z , and so it does not simply factor out of the z integral in (E2). Nonetheless, the partial wave inside the integrand grows exponentially, and therefore the integral in (E2) is dominated by the region where $z \sim z_{\min}$ and therefore

$$k_{\ell J}(v, s) \sim \frac{2}{\pi} \frac{s(z_{\min} - 1) + v - 4z_{\min}}{s - 4} \times P_J(x(v, t_{\min})) k_{\ell}^{\text{inn}}(s, v), \quad (\text{E10})$$

with

$$k_{\ell}^{\text{inn}}(s, v) \equiv P_{\ell}(z_{\min}) K(v, s, t_{\min}; t_0), \quad (\text{E11})$$

and $t_{\min} = t(z_{\min}) = -\frac{1}{2}(s-4)(1-z_{\min})$. Using (E1) and again the fact that the partial wave in the integrand grows exponentially with J , we obtain¹⁷

$$\bar{w}_J(v) \sim \frac{2(\mu_e^2 - v)^3}{\pi J^2 (\mu_e^2 - 4)^2} P_J(x(v, 2 - \frac{\mu_e^2}{2})) \Phi(v),$$

where

$$\Phi(v) \equiv K(v, \mu_e^2, 2 - \frac{\mu_e^2}{2}; t_0) \times \left[\sum_{n=0}^{\lfloor L/2 \rfloor} w_{2n}(\mu_e^2) P_{2n}(0) - \sum_{n=0}^{\lfloor L/2-1 \rfloor} \frac{1}{2} w_{2n+1}(2 + \frac{\mu_e^2}{2}) P_{2n+1}(-1) \right]. \quad (\text{E12})$$

The sign constraint on \bar{w}_J now becomes a sign constraint on the J -independent function $\Phi(v)$. It dependence on v only through the kernel, while the dual parameters only enter at the points $w_{2n}(\mu_e^2)$ and $w_{2n+1}(2 + \frac{\mu_e^2}{2})$. Hence, the sign constraint can only be satisfied over a region in which the kernel

$$K(v, \mu_e^2, 2 - \frac{\mu_e^2}{2}; t_0) = \frac{(\mu_e^2 - t_0)(\mu_e^2 - 4 + 2t_0)}{(v - t_0)(\mu_e^2 - v)(2v + \mu_e^2 - 4)} \times \frac{4v - 4 - \mu_e^2}{\mu_e^2 + 4 - 2v - 2t_0}, \quad (\text{E13})$$

has a fixed sign. The first factor is clearly positive. We then demand that the second factor has a fixed sign in the range $v \in [4, v_c]$. At $v = v_c$ this factor reduces to the manifestly positive value $\frac{3}{8}(\mu_e^2 + 4)$. At $v = 4$ it takes the form $(12 - \mu_e^2)/(\mu_e^2 - 4/3)$. Hence, for the sign constraint (B6) to be feasible at large spin, we are forced to take $\mu_e^2 \leq 12$ and $\mu_o^2 \leq 8$ correspondingly. This constraint on the regime of the dual problem comes from the kernel and is independent of the choice t_0 . Moreover, it can be shown to hold in any dimension $d \geq 3$.

To summarize, provided that $\mu_e^2 \leq 12$, the large J sign constrain in the inner region reduce to a corresponding

¹⁷Note that t_{\min} depends on s .

J and v independent sign constraint on the sum

$$\sum_{n=0}^{\lfloor L/2 \rfloor} \frac{(-1)^n \Gamma(n + \frac{1}{2})}{\Gamma(n+1)} w_{2n}(\mu_e^2) + \sum_{n=0}^{\lfloor L/2-1 \rfloor} \frac{1}{2} w_{2n+1}(2 + \frac{\mu_e^2}{2}), \quad (\text{E14})$$

where we have used the explicit value of the Legendre function.

Appendix F: Constraints from the threshold

For intermediate spins we have also imposed the $\bar{w}_J(v)$ sign constrain (25) near the two-particle threshold up to some cutoff higher than J_{\max} . In this limit, the constraint slightly simplifies as we now explain.

As $v \rightarrow 4^+$ the argument of the partial waves in (20) blows up and we can approximate these polynomials by their leading power

$$\lim_{x \rightarrow \infty} P_J^{(d)}(x) = {}_2F_1\left(\frac{1-J}{2}, -\frac{J}{2}, \frac{d-3}{2}, 1\right) x^J [1 + \mathcal{O}(1/x)]. \quad (\text{F1})$$

Correspondingly, in this limit we have

$$\bar{w}_J(v) \sim \frac{\mathcal{N}_d n_J^{(d)}}{\pi(v-4)^J} {}_2F_1\left(\frac{1-J}{2}, -\frac{J}{2}, \frac{d-3}{2}, 1\right) \times \left(\sum_{n=0}^{\lfloor L/2 \rfloor} \int_4^{\mu_e^2} ds w_{2n} k_{2n,J}^{\text{thr}} - \sum_{n=0}^{\lfloor L/2-1 \rfloor} \int_4^{\mu_o^2} \frac{w_{2n+1}}{2} k_{2n+1,J}^{\text{thr}} \right), \quad (\text{F2})$$

where

$$k_{\ell,J}^{\text{thr}} = \int_{z_{\min}}^1 dz P_{\ell}^{(d)}(z) (1-z^2)^{\frac{d-4}{2}} \times [(4t_0)^J K(4, t(z), t_0; s_0) + (4t(z))^J K(4, s, t(z); t_0)]. \quad (\text{F3})$$

Appendix G: Dual Numerics

In this appendix we give more details about the numerical implementation.

We choose the following parametrization for the dual variables

$$X_J(s) = \frac{\alpha^J \delta_{J,0}}{\sqrt{s-4}} + \sum_{n=0}^{N_X(J)} \beta_n^J \text{Ch}_n\left(1 + \frac{2(s-\mu_e^2)}{\mu_e^2-4}\right),$$

$$w_{\ell}(s) = \sum_{n=0}^{N_w(\ell)} w_n^{\ell} \text{Ch}_n\left(1 + \frac{2(s-\mu_e^2)}{\mu_e^2-4}\right), \quad (\text{G1})$$

where $\alpha^0, \beta_n^J, w_n^{\ell}$ are free parameters with J even and ℓ any positive integer and Ch_n are the Chebyshev polynomials. The square root singularity at threshold for X_0 is allowed by the general threshold expansion of the dual constraints and by the regularity of the dual objective, see (D2). It turns out to help the convergence for the maximum coupling problem.

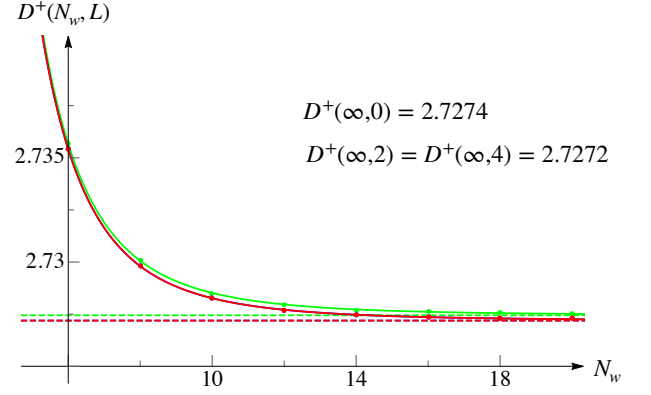


FIG. 4. Minimum value of the dual objective $D^+(4/3, 4/3)$ (B3) for the maximum coupling problem as a function of N_w and L . Different colors correspond respectively to $L = 0$ (green), $L = 2$ (blue) and $L = 4$ (red). The blue curve is covered by the red one as the bound does improve anymore by increasing L . The addition of odd dual variables w_{2n+1} has no effect on the bound. The dashed lines represent the corresponding extrapolations to $L \rightarrow \infty$. Our best bound $g_0 \leq 2.7272 < 2.75$ improves the one found in [26], but is still bigger than the one obtained by the primal [6] and the dual of [27].

The dual unitarity constraints (24) imply that $X_J(s) \geq 0$. The parametrization in (G1) is not manifestly positive and it is convenient to supplement the dual constraints with the necessary conditions $X_J(s_i) \geq 0$ for some very refined grid $\{s_i\}$.¹⁸

To run the numerics we choose the following strategy. We fix $N_X(J)$ to some high value, for instance, $N_X(J) = 40$ and we slowly increase $N_w(\ell)$. The reason is that although we need to impose the linear constraints (B6) for all J 's, when running the numerics we need to introduce a cutoff J_{\max} . The functionals \bar{w}_J depend only on $N_w(\ell)$, and for any fixed $N_w(\ell)$ we want to make sure that J_{\max} is large enough to prevent dual constraints violations. To further simplify the analysis we keep $N_w(2n+1) = 4$ fixed. Notice that the w_{2n+1} only enters in the optimization problem integrated against some kernel. Indeed, w_{2n+1} can wildly oscillate without changing \bar{w}_J . We found empirically that just increasing $N_w(2n+1)$ makes J_{\max} convergence harder without improving the bound significantly.

The best bound is obtained integrating on the largest possible region in s , therefore in our numerics we set $\mu_e^2 = 12$ and $\mu_o^2 = 8$ – see Appendix E 2. We compute the \bar{w}_J functionals analytically: the integrated expressions are lengthy but simple as they contain at most logarithms and dilogarithms.

We map both the region $4 < v < \mu_e^2$ and the region $\mu_e^2 < v$ to the interval $[-1, 1]$ and there we impose the

¹⁸It is possible to trivialize this necessary condition by parametrizing $X_0(s)$ in terms of Bernstein polynomials of the form $(1-x)^k(1-x^j)$. However, we have found such an expansion to converge slowly.

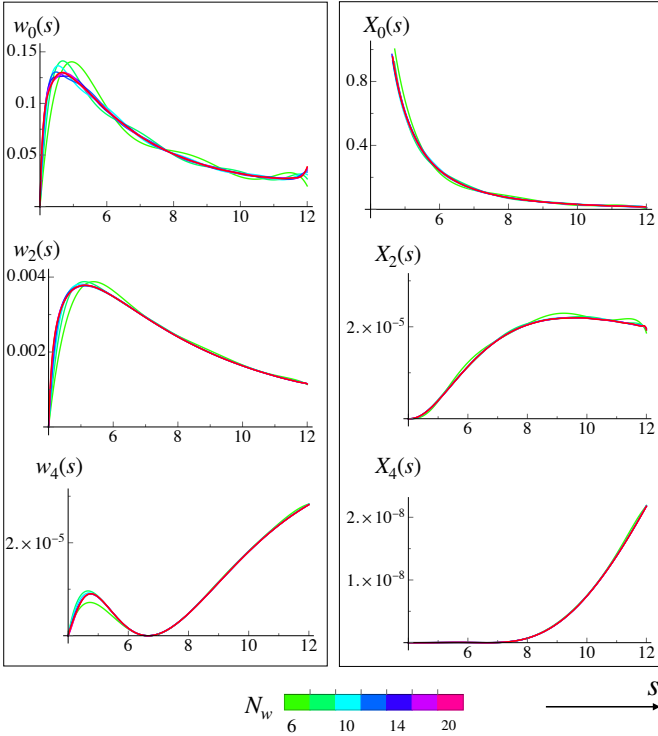


FIG. 5. In the left panel we show the dual dispersion variables w_{2n} for $n = 0, 1, 2$. On the right, we show the unitarity dual variables. The dual objective D^+ is obtained by summing the areas below the X_J curves. We see how small is the contribution to the bound coming from the higher spins. Convergence in N_w is also achieved fast as the various curves tend to overlap by increasing N_w .

dual constraints on a Chebyshev grid with respectively 500 and 80 points. We now discuss our numerical findings in turn for the maximum and minimum coupling problems.

1. Maximum coupling dual problem

We start with the maximum coupling problem since it turns out to be one of the simplest S-matrix Bootstrap problems. The bound converges already when $L = 0$ and adding higher spin constraints does not improve it significantly. We observe that just imposing the $\bar{w}_2 \geq 0$ together with the large J constraints is sufficient to make all the $\bar{w}_J \geq 0$ constraints with $J > 2$ automatically satisfied. Moreover, turning on the odd w_{2n+1} 's has an almost zero impact on the bound.

In figure 4 we plot the value of the minimum value of the dual objective (B3) $D^+(4/3, 4/3)$, that we simply denote by D^+ , as a function of N_w for $L = 0, 2, 4$ respectively in green, blue and red (the blue points are invisible since overlap with the red ones).¹⁹ The dashed lines are

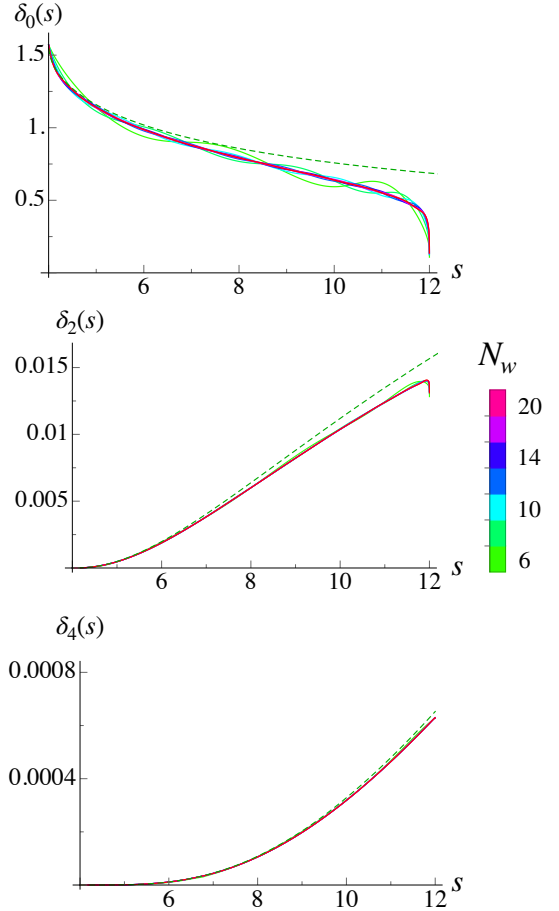


FIG. 6. Phase shifts $\delta_\ell(s) = \frac{1}{2i} \log S_\ell(s)$ for the first few spins as a function of s . In green dashed we plot the primal phase shifts for our best numerics $N_{\max} = 10$, $L_{\max} = 10$. Solid lines in color gradient are obtained from the dual numerics with $L = 4$ and different N_w . It is not surprising that primal and dual curves agree as the relative duality gap is relatively small $\Delta_{\text{gap}} = 2 \frac{|g_0 - D^+|}{g_0 + D^+} = 0.02$.

the power-law extrapolations for $N_w \rightarrow \infty$ with the extrapolated value reported in the figure. Taking the best value we conclude that $g_0 \leq 2.7272$.

In figure 5 we show how the various dual variables converge as we increase N_w from $N_w = 6$ to $N_w = 20$ in color gradient for the $L = 4$ numerics. On the left panels we show the dual dispersive variables $w_{2n}(s)$ which depend on N_w . In the right panels, we plot the dual unitarity variables X_J : the area below those curves contribute to the dual objective D^+ and from the plot is clear that almost the whole contribution to the bound comes from the spin-0 partial wave only.

We also checked numerically that dual unitarity $\det \Lambda_J^+(s) \approx 0$. According to the discussion in Appendix D, this allows us to extract reliably the phase shifts using (D1). In figure 6 we plot the real phase shifts for $J = 0, 2, 4$ using the data obtained with $L = 4$ as function of N_w . The green dashed lines represent the primal phase shifts obtained with $N_{\max} = 5$ and $L_{\max} = 10$.

¹⁹We keep $N_w(\ell)$ the same for all even ℓ .

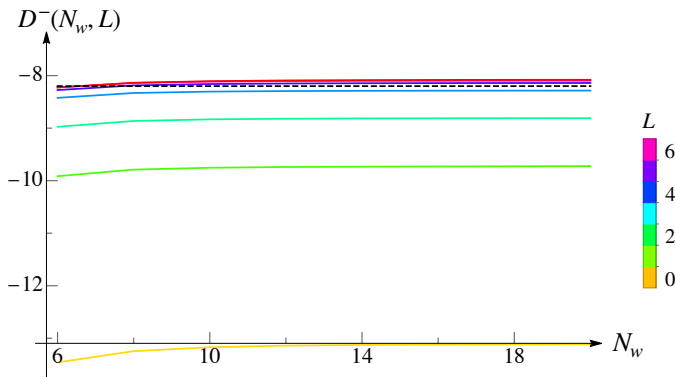


FIG. 7. Dual objective $D^-(4/3, 4/3)$ for the minimum coupling problem as a function of N_w . Different colors correspond to different values of L . Here we see that the effect of the odd w_{2n+1} is important for the convergence of the bound. The black dashed line represents the bound obtained in [26]. Also in this case the bound we get improves the old results and is the best rigorous bound obtained so far: $g_0 \geq -8.08$.

The phase shifts for $J > 0$ are all small and positive with positive scattering length (the slope at threshold), which is compatible with an extremal amplitude dominated by the spin 0 partial wave, where the higher spins are barely excited.

2. Minimum coupling dual problem

The minimum coupling problem is one of the hardest S -matrix Bootstrap problems since the corresponding optimal amplitude maximizes the total cross-section, see section II C. This difficulty turns into a much slower convergence of the dual problem in comparison to the one for the maximum coupling. In figure 7 we study the maximum of the dual-functional $D^-(4/3, 4/3)$, denoted shortly as D^- , as a function of N_w for different values of L .

The dashed black line corresponds to the bound obtained by Lopez and Mennessier [26] $g_0 \geq -8.2$. Taking the bound obtained with $L = 6$ and $N_w = 20$ and extrapolating for $J_{\max} \rightarrow \infty$ we can claim that $g_0 \geq -8.08$. The difference Δ between the extrapolated value and the bound we get for the higher value of $J_{\max} = 26$ is $\Delta = 4 \times 10^{-3}$. The (small) dependence on J_{\max} means we still have some dual constraint violations. An inspection shows that the violations happen in the outer region $v \geq v_c$ in some intermediate range of energies that depend on the spin J . It would be interesting to estimate this region and prevent these violations by adding some fine-tuned constraints. However, as we said, their effect on the bound is very small.

Another difference w.r.t the maximum coupling problem is that every time we add an odd spin constraint the bound changes by a comparable amount to the one generated by adding the even ones, see figure 7.

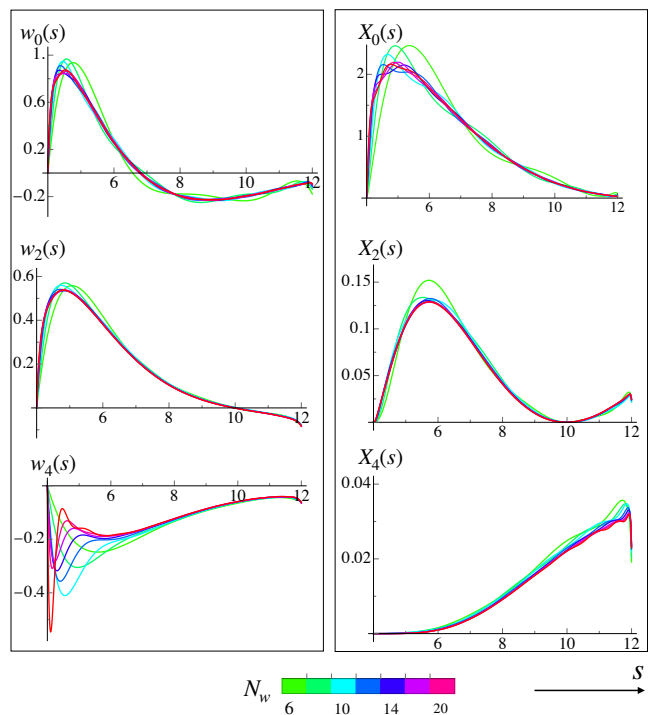


FIG. 8. Similarly to figure 5, on the left panel we have the dual dispersion variables w_{2n} for $n = 0, 1, 2$, and on the right the unitarity dual variables. The dual objective D^- is obtained by summing the areas below the X_J curves with a negative sign. In this case, spin-2 and spin-4 contribute respectively to the 5% and 1% of the bound. Convergence in N_w is also achieved for all dual variables, but w_4 . We have observed that higher spins tend to stabilize as we increase L . Allowing for a more general threshold behavior might also help w_4 to stabilize. We leave this problem for the future as it does not affect the numerical stability of the bound, nor of the physical phase shifts.

In figure 8 we show the dual variables w_{2n} (left panels) and X_{2n} (right panels) up to $n = 2$. Again, it is worth noticing how the dual variables for this problem have a non-trivial higher spin structure compared to the maximum coupling case, figure 5. The contribution to the dual objective coming from X_2 and X_4 accounts respectively for the 5% and 1% of the bound. Moreover, though the dual variable w_4 does not seem to converge yet in N_w , we observe that X_4 is stable. From our preliminary explorations it seems that as we add higher spin waves, the lower spins tend to stabilize. We expect that this will happen to the spin-4 dual variable if we were to increase further L . We leave this study to the future.

Finally in figure 9 we compare primal (dashed-greed) and dual (color gradient) physical phase shifts for spin $\ell = 0, 2, 4$. In this case, the ratio between the duality gap and the bound is still large. Therefore, it does not come as a surprise that the phase shifts are different. This difference is more pronounced as we go to higher spins and energies. The spin-0 phase shift δ_0 agrees nicely. In particular, this phase shift and the corresponding scattering

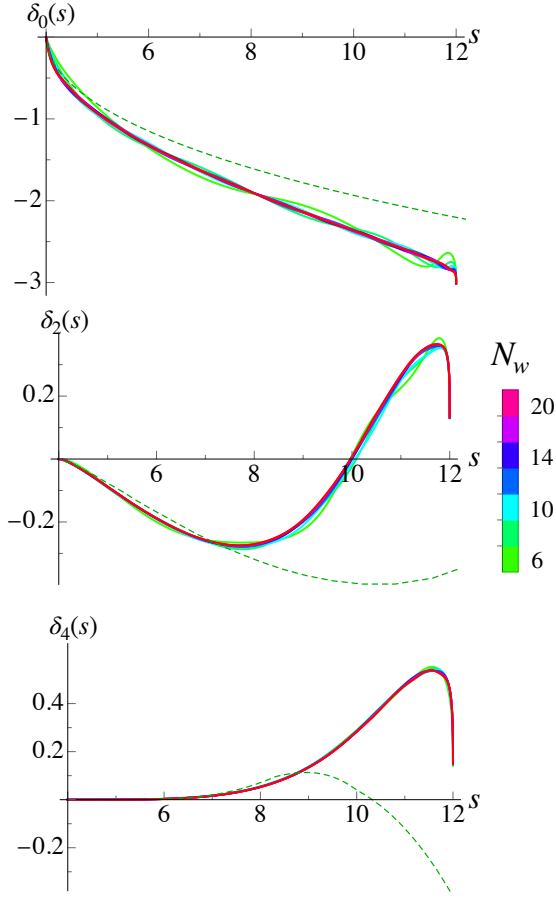


FIG. 9. Phase shifts $\delta_\ell(s) = \frac{1}{2i} \log S_\ell(s)$ for the first few spins as a function of s of the amplitude that minimizes the quartic coupling. In green dashed we plot the primal phase shifts for our best numerics $N_{\max} = 20$, $L_{\max} = 22$. Solid lines in color gradient are obtained from the dual numerics with $L = 4$ and different N_w . In this case, primal and dual differ significantly, especially for higher spins. The duality gap is also relatively big $\Delta_{\text{gap}} = 2 \frac{|g_0 - D^-|}{|g_0 + D^-|} = 0.26$. One reason for this discrepancy comes from primal numerics as both the bound and unitarity saturation are still far from being attained. Nonetheless, the threshold physics is compatible, and we do expect they will agree more as the duality gap shrinks – see also figure 3.

length are negative for both primal and dual problems. For spin-2 and spin-4 the threshold behavior seems to agree, but at intermediate energies, they differ significantly. In this case, we observe that unitarity is not well saturated for primal both for spin-2 and spin-4. Hence, it might be useful to further improve the primal and achieve better convergence before drawing any conclusion.

As a last comment, it seems that the spin-2 scattering length for the minimum coupling problem is nega-

tive, while for spin-4 and higher becomes positive. This seems to be in contrast with the expectation coming from Froissart-Gribov representation that would suggest a positive spin-2 scattering length [55].

Appendix H: Threshold unitarity

In this appendix, we study the constraints that come from threshold unitarity in a $3 + 1$ dimensional gapped theory and make a connection to our numerical results.²⁰

We assume a threshold behavior of the form

$$T(s, t, u) = -\alpha \left(\frac{1}{\sqrt{4-s}} + \frac{1}{\sqrt{4-t}} + \frac{1}{\sqrt{4-u}} \right) + a_0 + ib_0(\sqrt{s-4} + \sqrt{t-4} + \sqrt{u-4}). \quad (\text{H1})$$

Its projection onto the spin-0 partial wave is

$$S_0(s) = 1 - \frac{\alpha}{32\pi} + i\sqrt{s-4} \frac{a_0 - 4b_0 - \alpha}{32\pi} + \mathcal{O}(s-4). \quad (\text{H2})$$

Expanding the elastic unitarity condition for $s \rightarrow 4^+$ implies that

$$\alpha = 0 \quad \text{or} \quad \alpha = 64\pi. \quad (\text{H3})$$

and

$$b_0 = (a_0 - \alpha)/4. \quad (\text{H4})$$

For $\alpha = 64\pi$, the amplitude has a pole at threshold and the spin-0 phase shift reads

$$\delta_0(s) = \pm \frac{\pi}{2} + \frac{1}{16} \left(2 \mp \sqrt{100 - \frac{a_0}{\pi}} \right) \sqrt{s-4} + \dots \quad (\text{H5})$$

It starts at $\pi/2$ and from its slope, we can extract the coefficient a_0 . In particular, the reality of the phase in the elastic unitarity region implies that $a_0 \leq 100\pi$. This is the behavior observed in figure 3 (top) and figure 6 for the maximum coupling problem.

For $\alpha = 0$ we get

$$\delta_0(s) = \frac{1}{16} \left(-2 \pm \sqrt{4 + \frac{a_0}{\pi}} \right) \sqrt{s-4} + \dots, \quad (\text{H6})$$

and the amplitude approach the constant a_0 at threshold, which is called *scattering length*. This is the behavior observed in figure 3 (bottom), and figure 9 for the minimum coupling.

The scattering length a_0 controls the time delay of the waves in the non-relativistic limit. A negative scattering length would signal a time advance. It is therefore expected to be bounded from below. Indeed, the reality of the phase now implies that $a_0 \geq -4\pi$.

²⁰See [38] for a general analysis.

-
- [1] Miguel F. Paulos, Joao Penedones, Jonathan Toledo, Balt C. van Rees, and Pedro Vieira, “The S-matrix bootstrap II: two dimensional amplitudes,” *JHEP* **11**, 143 (2017), arXiv:1607.06110 [hep-th].
 - [2] Miguel F. Paulos, Joao Penedones, Jonathan Toledo, Balt C. van Rees, and Pedro Vieira, “The S-matrix bootstrap. Part III: higher dimensional amplitudes,” *JHEP* **12**, 040 (2019), arXiv:1708.06765 [hep-th].
 - [3] N. Doroud and J. Elias Miró, “S-matrix bootstrap for resonances,” *JHEP* **09**, 052 (2018), arXiv:1804.04376 [hep-th].
 - [4] Yifei He, Andrew Irrgang, and Martin Kruczenski, “A note on the S-matrix bootstrap for the 2d $O(N)$ bosonic model,” *JHEP* **11**, 093 (2018), arXiv:1805.02812 [hep-th].
 - [5] Lucía Córdova and Pedro Vieira, “Adding flavour to the S-matrix bootstrap,” *JHEP* **12**, 063 (2018), arXiv:1805.11143 [hep-th].
 - [6] Miguel F. Paulos and Zechuan Zheng, “Bounding scattering of charged particles in $1+1$ dimensions,” *JHEP* **05**, 145 (2020), arXiv:1805.11429 [hep-th].
 - [7] Alexandre Homrich, João Penedones, Jonathan Toledo, Balt C. van Rees, and Pedro Vieira, “The S-matrix Bootstrap IV: Multiple Amplitudes,” *JHEP* **11**, 076 (2019), arXiv:1905.06905 [hep-th].
 - [8] Joan Elias Miró, Andrea L. Guerrieri, Aditya Hebbar, João Penedones, and Pedro Vieira, “Flux Tube S-matrix Bootstrap,” *Phys. Rev. Lett.* **123**, 221602 (2019), arXiv:1906.08098 [hep-th].
 - [9] Lucía Córdova, Yifei He, Martin Kruczenski, and Pedro Vieira, “The $O(N)$ S-matrix Monolith,” *JHEP* **04**, 142 (2020), arXiv:1909.06495 [hep-th].
 - [10] Carlos Bercini, Matheus Fabri, Alexandre Homrich, and Pedro Vieira, “S-matrix bootstrap: Supersymmetry, Z_2 , and Z_4 symmetry,” *Phys. Rev. D* **101**, 045022 (2020), arXiv:1909.06453 [hep-th].
 - [11] Andrea L. Guerrieri, Alexandre Homrich, and Pedro Vieira, “Dual S-matrix Bootstrap I: 2D Theory,” (2020), arXiv:2008.02770 [hep-th].
 - [12] Martin Kruczenski and Harish Murali, “The R-matrix bootstrap for the 2d $O(N)$ bosonic model with a boundary,” *JHEP* **04**, 097 (2021), arXiv:2012.15576 [hep-th].
 - [13] Andrea L. Guerrieri, Joao Penedones, and Pedro Vieira, “Bootstrapping QCD Using Pion Scattering Amplitudes,” *Phys. Rev. Lett.* **122**, 241604 (2019), arXiv:1810.12849 [hep-th].
 - [14] Anjishnu Bose, Parthiv Haldar, Aninda Sinha, Pritish Sinha, and Shaswat S. Tiwari, “Relative entropy in scattering and the S-matrix bootstrap,” (2020), arXiv:2006.12213 [hep-th].
 - [15] Andrea Guerrieri, Joao Penedones, and Pedro Vieira, “S-matrix Bootstrap for Effective Field Theories: Massless Pions,” (2020), arXiv:2011.02802 [hep-th].
 - [16] Aditya Hebbar, Denis Karateev, and Joao Penedones, “Spinning S-matrix Bootstrap in 4d,” (2020), arXiv:2011.11708 [hep-th].
 - [17] Anjishnu Bose, Aninda Sinha, and Shaswat S. Tiwari, “Selection rules for the S-Matrix bootstrap,” (2020), arXiv:2011.07944 [hep-th].
 - [18] Andrea Guerrieri, Joao Penedones, and Pedro Vieira, “Where is String Theory?” (2021), arXiv:2102.02847 [hep-th].
 - [19] David Poland, Slava Rychkov, and Alessandro Vichi, “The Conformal Bootstrap: Theory, Numerical Techniques, and Applications,” *Rev. Mod. Phys.* **91**, 015002 (2019), arXiv:1805.04405 [hep-th].
 - [20] David Simmons-Duffin, “A Semidefinite Program Solver for the Conformal Bootstrap,” *JHEP* **06**, 174 (2015), arXiv:1502.02033 [hep-th].
 - [21] Walter Landry and David Simmons-Duffin, “Scaling the semidefinite program solver SDPB,” (2019), arXiv:1909.09745 [hep-th].
 - [22] C. Lopez, “A Lower Bound to the $\pi^0 \pi^0$ S-Wave Scattering Length,” *Nucl. Phys. B* **88**, 358–364 (1975).
 - [23] C. Lopez, “Rigorous Lower Bounds for the $\pi \pi$ p-Wave Scattering Length,” *Lett. Nuovo Cim.* **13**, 69 (1975).
 - [24] C. Lopez and G. Mennessier, “A New Absolute Bound on the $\pi^0 \pi^0$ S-Wave Scattering Length,” *Phys. Lett. B* **58**, 437–441 (1975).
 - [25] B. Bonnier, C. Lopez, and G. Mennessier, “Improved Absolute Bounds on the $\pi^0 \pi^0$ Amplitude,” *Phys. Lett. B* **60**, 63–66 (1975).
 - [26] C. Lopez and G. Mennessier, “Bounds on the $\pi^0 \pi^0$ Amplitude,” *Nucl. Phys. B* **118**, 426–444 (1977).
 - [27] Yifei He and Martin Kruczenski, “S-matrix bootstrap in $3+1$ dimensions: regularization and dual convex problem,” (2021), arXiv:2103.11484 [hep-th].
 - [28] Joan Elias Miró and Andrea Guerrieri, “Dual EFT Bootstrap: QCD flux tubes,” (2021), arXiv:2106.07957 [hep-th].
 - [29] S. Boyd and L. Vandenberghe, *Convex Optimization*, Cambridge Univ. Press (2004).
 - [30] D. Luenberger, *Optimization by Vector Space Methods*, 1997, 1ed, John Wiley and Sons, Inc.
 - [31] D. Bertsekas, A. Nedic, and A. Ozdaglar, *Convex Analysis and Optimization*, MIT, 2003.
 - [32] Andre Martin, “Extension of the axiomatic analyticity domain of scattering amplitudes by unitarity. 1.” *Nuovo Cim. A* **42**, 930–953 (1965).
 - [33] Andre Martin, “Extension of the axiomatic analyticity domain of scattering amplitudes by unitarity. 2.” *Nuovo Cim. A* **44**, 1219 (1966).
 - [34] S. M. Roy, “Exact integral equation for pion pion scattering involving only physical region partial waves,” *Phys. Lett. B* **36**, 353–356 (1971).
 - [35] G. Auberson and N. N. Khuri, “Rigorous parametric dispersion representation with three-channel symmetry,” *Phys. Rev. D* **6**, 2953–2966 (1972).
 - [36] G. Mahoux, S. M. Roy, and G. Wanders, “Physical pion pion partial-wave equations based on three channel crossing symmetry,” *Nucl. Phys. B* **70**, 297–316 (1974).
 - [37] Andrea L. Guerrieri and Amit Sever, “work in progress,” .
 - [38] Miguel Correia, Amit Sever, and Alexander Zhiboedov, “An Analytical Toolkit for the S-matrix Bootstrap,” (2020), arXiv:2006.08221 [hep-th].
 - [39] Stanley O. Aks, “Proof that Scattering Implies Production in Quantum Field Theory,” *J. Math. Phys.* **6**, 516–532 (1965).
 - [40] G. Colangelo, J. Gasser, and H. Leutwyler, “ $\pi\pi$ scattering,” *Nucl. Phys. B* **603**, 125–179 (2001), arXiv:hep-ph/0103088.
 - [41] Sebastian Mizera, “Bounds on Crossing Symmetry,”

- Phys. Rev. D **103**, 081701 (2021), arXiv:2101.08266 [hep-th].
- [42] Sebastian Mizera, “Crossing Symmetry in the Planar Limit,” (2021), arXiv:2104.12776 [hep-th].
 - [43] G. Auberson and L. Epele, “A Tool for Extending the Analyticity Domain of Partial Wave Amplitudes and the Validity of Roy-Type Equations,” *Nuovo Cim. A* **25**, 453 (1975).
 - [44] G. Auberson and S. Ciulli, “A Set of Integral Equations for Pion Pion Scattering Valid at All Energies,” *Nuovo Cim. A* **44**, 549 (1978).
 - [45] Aninda Sinha and Ahmadullah Zahed, “Crossing Symmetric Dispersion Relations in QFTs,” (2020), arXiv:2012.04877 [hep-th].
 - [46] Rajesh Gopakumar, Aninda Sinha, and Ahmadullah Zahed, “Crossing Symmetric Dispersion Relations for Mellin Amplitudes,” (2021), arXiv:2101.09017 [hep-th].
 - [47] Nima Arkani-Hamed, Tzu-Chen Huang, and Yu-Tin Huang, “The EFT-Hedron,” *JHEP* **05**, 259 (2021), arXiv:2012.15849 [hep-th].
 - [48] Michael B. Green and Congkao Wen, “Superstring amplitudes, unitarity, and Hankel determinants of multiple zeta values,” *JHEP* **11**, 079 (2019), arXiv:1908.08426 [hep-th].
 - [49] Brando Bellazzini, Joan Elias Miró, Riccardo Rattazzi, Marc Riembau, and Francesco Riva, “Positive Moments for Scattering Amplitudes,” (2020), arXiv:2011.00037 [hep-th].
 - [50] Andrew J. Tolley, Zi-Yue Wang, and Shuang-Yong Zhou, “New positivity bounds from full crossing symmetry,” (2020), arXiv:2011.02400 [hep-th].
 - [51] Simon Caron-Huot and Vincent Van Duong, “Extremal Effective Field Theories,” *JHEP* **05**, 280 (2021), arXiv:2011.02957 [hep-th].
 - [52] Simon Caron-Huot, Dalimil Mazac, Leonardo Rastelli, and David Simmons-Duffin, “Sharp Boundaries for the Swampland,” (2021), arXiv:2102.08951 [hep-th].
 - [53] Zvi Bern, Dimitrios Kosmopoulos, and Alexander Zhiboedov, “Gravitational Effective Field Theory Islands, Low-Spin Dominance, and the Four-Graviton Amplitude,” (2021), arXiv:2103.12728 [hep-th].
 - [54] Sandipan Kundu, “Swampland Conditions for Higher Derivative Couplings from CFT,” (2021), arXiv:2104.11238 [hep-th].
 - [55] F. J. Yndurain, “Rigorous constraints, bounds, and relations for scattering amplitudes,” *Rev. Mod. Phys.* **44**, 645–667 (1972).